

# Understanding multi-view transformers

Michal Stary<sup>1\*</sup>, Julien Gaubil<sup>2\*</sup>, Ayush Tewari<sup>3</sup>, Vincent Sitzmann<sup>4</sup>

<sup>1</sup>TUM, <sup>2</sup>Claude Bernard University Lyon 1, <sup>3</sup>University of Cambridge, <sup>4</sup>MIT CSAIL

michal.stary@tum.de, gaubil.julien@gmail.com, at2164@cam.ac.uk, sitzmann@mit.edu

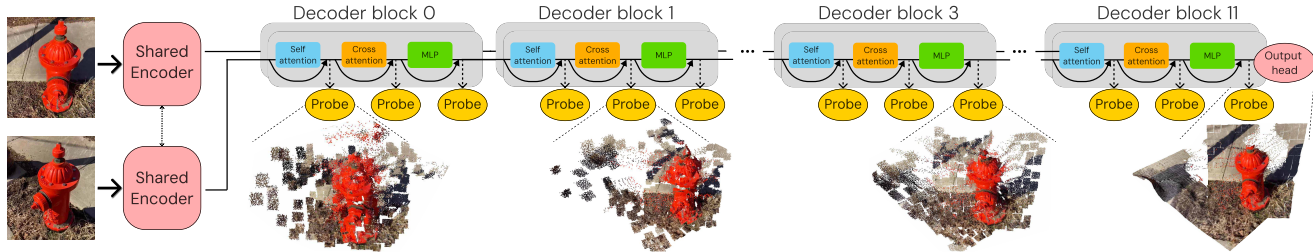


Figure 1. **Overview of our interpretability approach.** We probe the skip connections of DUS3R’s multi-view transformer decoder for pointmaps and visualize the gradual development of DUS3R’s latent 3D geometry, correspondence, and camera pose estimate.

## Abstract

Multi-view transformers such as DUS3R [59] are revolutionizing 3D vision by solving 3D tasks in a feed-forward manner. However, contrary to previous optimization-based pipelines, the inner mechanisms of multi-view transformers are unclear. Their black-box nature makes further improvements beyond data scaling challenging and complicates usage in safety- and reliability-critical applications. Here, we present an approach for probing and visualizing 3D representations from the residual connections of the multi-view transformers’ layers. In this manner, we investigate a variant of the DUS3R model, shedding light on the development of its latent state across blocks, the role of the individual layers, and suggest how it differs from methods with stronger inductive biases of explicit global pose. Finally, we show that the investigated variant of DUS3R estimates correspondences that are refined with reconstructed geometry. The code used for the analysis is available at <https://github.com/JulienGaubil/und3rstand>.

## 1. Introduction

Understanding and reconstructing 3D from video or multi-view images is a classic computer vision problem. Contrary to most other vision problems, 3D vision tasks are still often tackled with expert-crafted multi-step pipelines such as COLMAP [49].

Recently, the seminal work DUS3R [59] introduced a novel end-to-end deep learning framework that leverages multi-view transformers to predict pointmaps, recovering scene geometry in a feed-forward manner. Since its introduction, this framework has been successfully applied to perform 3D reconstruction [11, 31, 56, 58, 60], 3D understanding [20], and even 4D reconstruction [28, 64] from multi-view or video observations. Compared to conventional, optimization-based approaches, these feed-forward methods are fast and can solve underdetermined reconstruction problems, but lack mechanistic interpretability due to their black-box nature.

Meanwhile, model interpretability is an active research area in LLMs [12, 32, 41, 44] and recently also in vision [21, 22, 45, 66]. Methods falling under the umbrella of mechanistic interpretability, such as activation visualizations [19, 42, 54], transformer circuit analysis [18, 43], probing [1, 6, 17, 25], and activation intervention [24, 37, 38] have been used to understand the function of individual components of neural networks. Sparse Auto-Encoders (SAE) are a popular method to interpret the content of features [10, 30]. Unfortunately, applying SAEs to 3D multi-view transformers is challenging as they are focused on discrete concept disentanglement rather than recovering explicit spatial geometry.

For investigating the 3D-awareness of general vision models, researchers typically use learned probing for specific quantities such as depths, normals or correspondences [17, 36]. However, these probes have to date mostly been used to assess or extract 3D knowledge at a single layer or in

\*Equal contribution. Work done while a visiting student at MIT.

an aggregated manner, serving as means for evaluating and comparing models rather than interpretability. To the best of our knowledge, these tools have not yet been applied to multi-view transformers for 3D reconstruction.

Recent work [6, 13, 18, 23, 39], suggest that transformers carry a state through their skip connections, and this state is iteratively refined by every layer. Building on this observation, we analyze the spatial geometry of this state within a multi-view transformer by probing pointmaps from the individual patch features at every layer’s skip connection and sequentially visualize the resulting 3D representations.

In particular, we investigate a variant of the DUST3R model and demonstrate how it refines its internal state. Our analysis sheds light on the role of individual layers and indicates that the model is unlikely to utilize global pose information but relies heavily on correspondences.

## 2. Method

### 2.1. Preliminaries: DUST3R and pointmaps

DUST3R is a multi-view transformer trained to reconstruct 3D scenes from two input views [59]. For each pixel in both views, DUST3R outputs the corresponding 3D point expressed in the *first view* coordinate system, a 3D parameterization termed as *pointmap*. Predicting a pointmap for the first view requires estimating depth and intrinsics; the second view’s pointmap prediction requires estimating relative camera pose, depth, and intrinsics.

As depicted in Figure 1, DUST3R processes two input views using a shared ViT [16] encoder, followed by two view-specific decoders that communicate through cross-attention. The pointmaps are then regressed from both decoders using learnable heads applied to patch features output by the final transformer block of each decoder.

### 2.2. Probes

To understand the internal state as it propagates through the multi-view transformer, we train separate probes on the features after each skip connection in the decoder blocks, as illustrated in Figure 1. By doing so, we obtain three probes for each decoder block, corresponding to skip connections from its self-attention, cross-attention, and MLP layers.

### 2.3. Probing & visualizing pointmaps

We find that probing for pointmaps is particularly effective for inspecting and visualizing how the internal feature state evolves throughout the transformer.

The choice of pointmaps is motivated by their clear geometric interpretation, making them suitable for inspecting the spatial geometry inside the transformer features. Regressing pointmaps is also very similar to what DUST3R-like methods do and are trained for, which makes

these methods’ internal representations likely to be well-structured for this task. Finally, unlike other single-view parameterizations such as depth, pointmaps regress both views in the same scale, which is crucial for joint visualization due to an inherent scale-invariance of many multi-view transformers, as we ablate in Appendix A.

To faithfully observe the internal state, the capacity of the probe needs to be limited to prevent it from solving the task alone. We restrict the receptive field of our probes to operate only on *individual patch features*, without communication across patches, as shown in Figure 2. This restriction forces the probe to rely on local patch information, which is not sufficient to solve tasks requiring global reasoning across patches, such as estimating relative pose or joint geometry. This ensures that the probe output accurately reflects the content of the internal state of each patch.

After probing, we visualize the resulting pointmaps in 4D by sequentially iterating through the decoder layers and visualizing each 3D representation.

### 2.4. Implementation

We train independent pointmap probes for each probing location using the confidence-aware scale-invariant loss introduced in DUST3R (see Appendix C). We parametrize each probe as a five-layer MLP with ReLU activation functions. Notably, we found that using non-linear probes is essential to obtain interpretable pointmaps (see ablation in Appendix A). The probes are trained for 12 hours on an A100 GPU on 100,000 rendered images from the Habitat Matterport 3D [47] dataset.

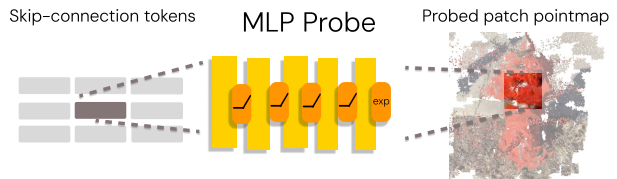


Figure 2. **Probing mechanism.** We train our probe to regress the patch of a pointmap from the corresponding vision transformer patch token.

## 3. Experiments

Through our experiments, we investigate four questions related to how DUST3R addresses the 3D reconstruction:

1. How does the internal state evolve across the decoder?
2. What is the role of individual layers of the network?
3. Does the network estimate and use global camera poses?
4. Does DUST3R utilize correspondences?

**Experimental setup.** We probe and analyze the DUST3R\_224\_linear pretrained checkpoint and



Figure 3. **Visualization of the pointmaps probed after skip connection across the decoder.** We show probes after self-attention (SA) layers at different blocks for two examples: hydrant (top) and chairs (bottom). The first view is tinted green, and the second view in red. We can observe the red-tinted patches as they move through 3D space toward their correct locations in a semi-rigid fashion.

use 1000 pairs from held-out scenes of Habitat Matterport 3D dataset to compute metrics. For qualitative results, we report selected real-world examples from generic and object-centric scenes that fall in the distribution of DUS3R.

### 3.1. How does the internal state evolve across decoder blocks?

In Figure 3, we show the state evolution for two different multi-view image pairs: a “simple” image pair, where the two views have significant overlap, and a “difficult” example where two views are captured by almost opposing camera views with few 3D points observed in both views. At the output of the shared encoder, the network already provides a strong geometric estimate of the first view, indicating that it has performed monocular depth and camera intrinsic estimation within the encoder.

Notably, in the simple hydrant example, the rotation component of the pose is already resolved after the first multi-view decoder block. Subsequent blocks then iteratively align the scale and refine the translation. In contrast, in the chairs example, which depicts similar chairs from opposing viewpoints, the correct pose emerges only after several iterations across decoder blocks.

This, along with other challenging examples shown in appendix (Fig. 10), suggests that the iterative nature of relative pose estimation may be a key factor behind the unexpected robustness of the DUS3R model family.

### 3.2. What is the role of individual layers?

After establishing the overall trend of iterative refinement across decoder blocks, we inspect the role of individual layers in detail. We observe that while patches of the first view act as a stable anchor, the patches of the second view are systematically transformed. See Appendix Fig. 12 for visual details. In particular, cross-attention tends to non-rigidly move a subset of patches from the second view (“transported patches”) towards selected patches in the

first view. Further investigation reveals that the transported patches generally consist of points observed in both views.

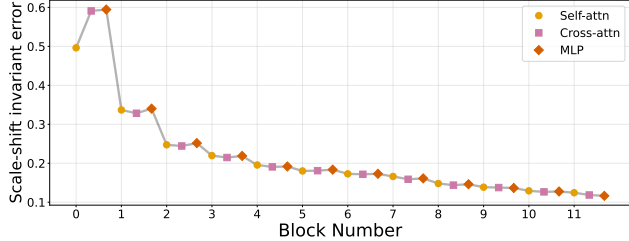
Self-attention, on the other hand, re-establishes intra-view geometry of the second-view pointmap. It acts mostly on the patches consisting primarily of monocular points, which were largely unaffected by the previous cross-attention (“leftover patches”). The self-attention *realigns the geometry of second view pointmap* by moving the leftover patches towards the transported patches.

We confirm the role of self-attention layers by extracting probed second-view pointmaps after each skip connection. We then align probed pointmaps with the ground-truth using Procrustes alignment [51], and compute the scale and shift-invariant error between the aligned predictions and the ground-truth pointmaps. The Procrustes alignment makes this error invariant to relative pose differences caused by imperfect alignment at intermediate steps (see Appendix Sec. E.2 for details). On average, the self-attention layers are responsible for *decreasing the aligned second-view error at the decoder input by 94%*. In contrast, the cross-attention layers increase this error by 11%, and the MLP layers increase it by 7%. See Figure 4 for per-block details.

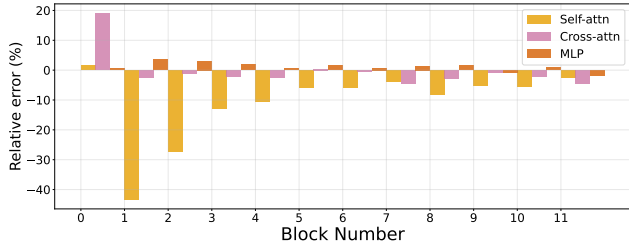
### 3.3. Does the network use global camera poses?

The problem of 3D reconstruction is naturally constrained by the assumption that every pair of pixels that depict the same 3D point is related by a global camera pose. Both classical [49] and recent [9, 46, 51, 57] methods leverage this rigid-body motion constraint to explicitly estimate the global relative camera pose between the two views and use it to reconstruct joint geometry. We investigate whether the increase in rigidity after self-attention arises from estimating and constraining a global pose transformation.

Such a pose would have to be synchronized across patches after each update. Therefore, we inspect the attention maps of self-attention layers to see if there are indications of such synchronization. We focus on the second de-



(a) **Scale and shift-invariant pointmap error** for the second view after Procrustes alignment, measured across blocks of the second-view decoder.



(b) **Layer-wise contribution to the reduction of scale and shift-invariant error** for the second view after Procrustes alignment. Relative error is reported with respect to the previous layer (in %).

Figure 4. **Layer-wise analysis of geometric refinement in the second view.** The poses of the predicted and ground-truth pointmaps are first aligned using a Procrustes solve. We then measure a scale and shift-invariant pointmap error to track the second view’s geometry refinement across the network. Most of the error reduction in the decoder is achieved by self-attention layers.

coder block, as it has the largest contribution to the restoration of the second view’s geometry, as shown in Figure 4. Out of the twelve attention heads, four attend to the same patches almost irrespective of the query. These patch tokens were identified in [14] and are possible candidates for storing and distributing the global pose information through the four heads mentioned above.

We perform an *attention knockout* intervention [24] on these heads and tokens (see Sec. G for details). As observed in Appendix Fig. 13, the ability to estimate pointmaps with the correct relative pose remains unchanged. This suggests that global pose information is not crucial for the self-attention functionality.

### 3.4. Does DUST3R utilize correspondences?

We find that DUST3R’s cross-attention layers align matching patches from different views. We investigate the cross-attention maps of the first decoder layer and find that five out of twelve heads attend to candidate corresponding patches (see Sec. F.2 for details). A similar ratio of *correspondence heads* is observed in the latter blocks of the decoder. When the correspondence search fails, or when no match exists due to occlusion or limited visual overlap, these correspondence heads tend to attend to one of the previously identified tokens [14], using them as a fallback.

**Correspondences turn from semantic to geometric.** We further investigate correspondence heads on the chairs example in Appendix Fig. 9. We observe that in early decoder blocks, correspondence head attention maps are consistent with *semantic* correspondences [8]—matching patches of the same appearance or semantics—while after some blocks, they are refined into *geometric* ones (matching patches of the same 3D point) [17].

**Measuring the refinement.** Building on the observation that correspondences are refined across decoder blocks, we extract correspondences from the correspondence heads identified above in cross-attention layers. We use a heuristic zero-shot estimator to quantify this refinement. See Sec. E.3 for details on the experimental setup. Following [17], we measure the 2D correspondence error and report the percentage of correspondences below a given distance threshold. Figure 5 shows the evolution of correspondence error across blocks, with a clear improvement from 40% correct correspondences at the input of the decoder to over 60% after the first six decoder blocks.

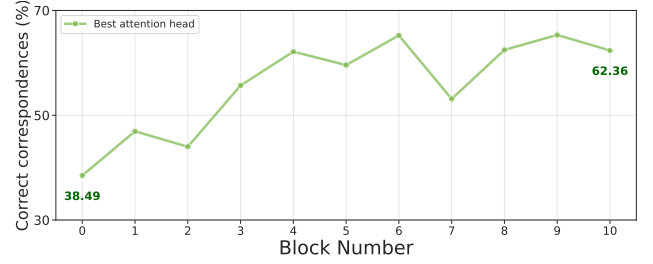


Figure 5. **Evolution of the percentage of valid correspondences** across the decoder blocks. Correspondences are considered valid if their 2D error is less than 16 pixels (1 patch). An improving trend is observed over the first six blocks.

We find that DUST3R has a strong notion of correspondences. Moreover, it refines these correspondences jointly with the internal geometry, highlighting an advantage over previous methods that depend on a fixed set of correspondences extracted externally prior to 3D reconstruction.

## 4. Conclusion

In this work, we have combined pointmap probing and visualization to investigate the spatial geometry of features computed by a multi-view transformer. Using our approach, we analyzed a variant of DUST3R. We have demonstrated how it iteratively refines geometry and identified the role of layer types and correspondences in this refinement.

Finally, we advocate that our approach is a useful investigation method for understanding the spatial geometry within multi-view transformers and should be considered as a good starting point to gain further insights about this interesting class of models.

**Acknowledgments** This work was supported by the National Science Foundation under Grant No. 2211259, by the Singapore DSTA under DST00OECL20300823 (New Representations for Vision, 3D Self-Supervised Learning for Label-Efficient Vision), by the Intelligence Advanced Research Projects Activity (IARPA) via Department of Interior/ Interior Business Center (DOI/IBC) under 140D0423C0075, by the Amazon Science Hub, and by the MIT-Google Program for Computing Innovation.

## References

[1] Guillaume Alain and Yoshua Bengio. Understanding intermediate layers using linear classifier probes. *arXiv*, 2018. 1, 9

[2] Sriram Balasubramanian, Samyadeep Basu, and Soheil Feizi. Decomposing and Interpreting Image Representations via Text in ViTs Beyond CLIP. In *NeurIPS*, 2024. 10

[3] Samyadeep Basu, Martin Grayson, Cecily Morrison, Bemira Nushi, Soheil Feizi, and Daniela Massiceti. Understanding Information Storage and Transfer in Multi-modal Large Language Models. In *NeurIPS*, 2024. 10

[4] David Bau, Jun-Yan Zhu, Hendrik Strobelt, Bolei Zhou, Joshua B. Tenenbaum, William T. Freeman, and Antonio Torralba. Visualizing and Understanding Generative Adversarial Networks. In *ICLR*, 2019. 9

[5] David Bau, Jun-Yan Zhu, Hendrik Strobelt, Agata Lapedriza, Bolei Zhou, and Antonio Torralba. Understanding the role of individual units in a deep neural network. *Proceedings of the National Academy of Sciences*, 2020. 9

[6] Nora Belrose, Zach Furman, Logan Smith, Danny Halawi, Igor Ostrovsky, Lev McKinney, Stella Biderman, and Jacob Steinhardt. Eliciting Latent Predictions from Transformers with the Tuned Lens. *arXiv*, 2023. 1, 2, 9

[7] Leonard Bereska and Efstratios Gavves. Mechanistic Interpretability for AI Safety - A Review. *TMLR*, 2024. 9

[8] Alexander C. Berg, Tamara L. Berg, and Jitendra Malik. Shape matching and object recognition using low distortion correspondences. In *CVPR*, 2005. 4

[9] Eric Brachmann, Jamie Wynn, Shuai Chen, Tommaso Cavallari, Áron Monszpart, Daniyar Turmukhambetov, and Victor Adrian Prisacariu. Scene Coordinate Reconstruction: Posing of Image Collections via Incremental Learning of a Relocalizer. In *ECCV*, 2024. 3, 9

[10] Trenton Bricken, Adly Templeton, Joshua Batson, Brian Chen, Adam Jermyn, Tom Conerly, Nick Turner, Cem Anil, Carson Denison, Amanda Askell, Robert Lasenby, Yifan Wu, Shauna Kravec, Nicholas Schiefer, Tim Maxwell, Nicholas Joseph, Zac Hatfield-Dodds, Alex Tamkin, Karina Nguyen, Brayden McLean, Josiah E Burke, Tristan Hume, Shan Carter, Tom Henighan, and Christopher Olah. Towards Monosemanticity: Decomposing Language Models With Dictionary Learning, 2023. <https://transformer-circuits.pub/2023/monosemantic-features/index.html>. Accessed: 2025-09-06. 1, 9

[11] Yohann Cabon, Lucas Stoffl, Leonid Antsfeld, Gabriela Csurka, Boris Chidlovskii, Jerome Revaud, and Vincent Leroy. MUS3R: Multi-view Network for Stereo 3D Reconstruction. In *CVPR*, 2025. 1

[12] Nick Cammarata, Shan Carter, Gabriel Goh, Chris Olah, Michael Petrov, Ludwig Schubert, Chelsea Voss, Ben Egan, and Swee Kiat Lim. Thread: Circuits, 2020. <https://distill.pub/2020/circuits>. Accessed: 2025-09-06. 1

[13] Guy Dar, Mor Geva, Ankit Gupta, and Jonathan Berant. Analyzing Transformers in Embedding Space. *arXiv*, 2023. 2, 9

[14] Timothée Darcet, Maxime Oquab, Julien Mairal, and Piotr Bojanowski. Vision Transformers Need Registers. In *ICLR*, 2024. 4, 9, 13

[15] Alexey Dosovitskiy and Thomas Brox. Inverting Visual Representations With Convolutional Networks. In *CVPR*, 2016. 9

[16] Alexey Dosovitskiy, Lucas Beyer, Alexander Kolesnikov, Dirk Weissenborn, Xiaohua Zhai, Thomas Unterthiner, Mostafa Dehghani, Matthias Minderer, Georg Heigold, Sylvain Gelly, Jakob Uszkoreit, and Neil Houlsby. An Image is Worth 16x16 Words: Transformers for Image Recognition at Scale. In *ICLR*, 2021. 2, 9

[17] Mohamed El Banani, Amit Raj, Kevis-Kokitsi Maninis, Abhishek Kar, Yuanzhen Li, Michael Rubinstein, Deqing Sun, Leonidas Guibas, Justin Johnson, and Varun Jampani. Probing the 3D Awareness of Visual Foundation Models. In *CVPR*, 2024. 1, 4, 8, 10, 12

[18] Nelson Elhage, Neel Nanda, Catherine Olsson, Tom Henighan, Nicholas Joseph, Ben Mann, Amanda Askell, Yuntao Bai, Anna Chen, Tom Conerly, Nova DasSarma, Dawn Drain, Deep Ganguli, Zac Hatfield-Dodds, Danny Hernandez, Andy Jones, Jackson Kernion, Liane Lovitt, Kamal Ndousse, Dario Amodei, Tom Brown, Jack Clark, Jared Kaplan, Sam McCandlish, and Chris Olah. A Mathematical Framework for Transformer Circuits, 2021. <https://transformer-circuits.pub/2021/framework/index.html>. Accessed: 2025-09-06. 1, 2

[19] Dumitru Erhan, Yoshua Bengio, Aaron Courville, and Pascal Vincent. Visualizing Higher-Layer Features of a Deep Network, 2009. Technical Report, University of Montreal. 1, 9

[20] Zhiwen Fan, Jian Zhang, Wenyan Cong, Peihao Wang, Renjie Li, Kairun Wen, Shijie Zhou, Achuta Kadambi, Zhangyang Wang, Danfei Xu, Boris Ivanovic, Marco Pavone, and Yue Wang. Large Spatial Model: End-to-end Unposed Images to Semantic 3D. In *NeurIPS*, 2024. 1, 9

[21] Yossi Gandelsman, Alexei A. Efros, and Jacob Steinhardt. Interpreting CLIP’s Image Representation via Text-Based Decomposition. In *ICLR*, 2024. 1, 10

[22] Yossi Gandelsman, Alexei A. Efros, and Jacob Steinhardt. Interpreting the Second-Order Effects of Neurons in CLIP. In *ICLR*, 2025. 1

[23] Mor Geva, Avi Caciularu, Kevin Ro Wang, and Yoav Goldberg. Transformer Feed-Forward Layers Build Predictions by Promoting Concepts in the Vocabulary Space. In *EMNLP*, 2022. 2, 9

[24] Mor Geva, Jasmijn Bastings, Katja Filippova, and Amir Globerson. Dissecting Recall of Factual Associations in

Auto-Regressive Language Models. In *EMNLP*, 2023. 1, 4, 9, 13

[25] Wes Gurnee, Neel Nanda, Matthew Pauly, Katherine Harvey, Dmitrii Troitskii, and Dimitris Bertsimas. Finding Neurons in a Haystack: Case Studies with Sparse Probing. *TMLR*, 2023. 1, 9

[26] Richard Hartley and Andrew Zisserman. *Multiple View Geometry in Computer Vision*. Cambridge University Press, second edition, 2003. 9

[27] Stanisław Jastrzebski, Devansh Arpit, Nicolas Ballas, Vikas Verma, Tong Che, and Yoshua Bengio. Residual Connections Encourage Iterative Inference. In *ICLR*, 2018. 9

[28] Linyi Jin, Richard Tucker, Zhengqi Li, David Fouhey, Noah Snavely, and Aleksander Holynski. Stereo4D: Learning How Things Move in 3D from Internet Stereo Videos. In *CVPR*, 2025. 1, 9

[29] Lubor Ladicky, Jianbo Shi, and Marc Pollefeys. Pulling things out of perspective. In *CVPR*, 2014. 8

[30] Tim Lawson, Lucy Farnik, Conor Houghton, and Laurence Aitchison. Residual Stream Analysis with Multi-Layer SAEs. In *ICLR*, 2025. 1, 9

[31] Vincent Leroy, Yohann Cabon, and Jerome Revaud. Grounding Image Matching in 3D with MAST3R. In *ECCV*, 2024. 1, 9

[32] Tom Lieberum, Senthooran Rajamanoharan, Arthur Conmy, Lewis Smith, Nicolas Sonnerat, Vikrant Varma, Janos Kramar, Anca Dragan, Rohin Shah, and Neel Nanda. Gemma Scope: Open Sparse Autoencoders Everywhere All At Once on Gemma 2. In *EMNLP BlackboxNLP Workshop*, 2024. 1, 9

[33] Ilya Loshchilov and Frank Hutter. Decoupled Weight Decay Regularization. In *ICLR*, 2019. 10

[34] Jie Ma, Yalong Bai, Bineng Zhong, Wei Zhang, Ting Yao, and Tao Mei. Visualizing and Understanding Patch Interactions in Vision Transformer. *IEEE Transactions on Neural Networks and Learning Systems*, 2024. 9

[35] Aravindh Mahendran and Andrea Vedaldi. Understanding Deep Image Representations by Inverting Them. In *CVPR*, 2015. 9

[36] Yunze Man, Shuhong Zheng, Zhipeng Bao, Martial Hebert, Liang-Yan Gui, and Yu-Xiong Wang. Lexicon3D: Probing Visual Foundation Models for Complex 3D Scene Understanding. In *NeurIPS*, 2024. 1, 10

[37] Kevin Meng, David Bau, Alex J Andonian, and Yonatan Belinkov. Locating and Editing Factual Associations in GPT. In *NeurIPS*, 2022. 1, 9

[38] Kevin Meng, Arnab Sen Sharma, Alex J Andonian, Yonatan Belinkov, and David Bau. Mass-Editing Memory in a Transformer. In *ICLR*, 2023. 1, 9

[39] Raul Molina. Traveling Words: A Geometric Interpretation of Transformers. *arXiv*, 2023. 2, 9

[40] Riku Murai, Eric Dexheimer, and Andrew J. Davison. MAST3R-SLAM: Real-Time Dense SLAM with 3D Reconstruction Priors. In *CVPR*, 2025. 9

[41] Neel Nanda, Lawrence Chan, Tom Lieberum, Jess Smith, and Jacob Steinhardt. Progress measures for grokking via mechanistic interpretability. In *ICLR*, 2023. 1

[42] Chris Olah, Alexander Mordvintsev, and Ludwig Schubert. Feature Visualization, 2017. <https://distill.pub/2017/feature-visualization>. Accessed: 2025-09-06. 1, 9

[43] Chris Olah, Nick Cammarata, Ludwig Schubert, Gabriel Goh, Michael Petrov, and Shan Carter. Zoom In: An Introduction to Circuits, 2020. <https://distill.pub/2020/circuits/zoom-in>. Accessed: 2025-09-06. 1

[44] Catherine Olsson, Nelson Elhage, Neel Nanda, Nicholas Joseph, Nova DasSarma, Tom Henighan, Ben Mann, Amanda Askell, Yuntao Bai, Anna Chen, Tom Conerly, Dawn Drain, Deep Ganguli, Zac Hatfield-Dodds, Danny Hernandez, Scott Johnston, Andy Jones, Jackson Kernion, Liane Lovitt, Kamal Ndousse, Dario Amodei, Tom Brown, Jack Clark, Jared Kaplan, Sam McCandlish, and Chris Olah. In-context Learning and Induction Heads. *arXiv*, 2022. 1

[45] Vedant Palit, Rohan Pandey, Aryaman Arora, and Paul Pu Liang. Towards Vision-Language Mechanistic Interpretability: A Causal Tracing Tool for BLIP. In *ICCV CLVL Workshop*, 2023. 1

[46] Linfei Pan, Dániel Baráth, Marc Pollefeys, and Johannes Lutz Schönberger. Global Structure-from-Motion Revisited. In *ECCV*, 2024. 3

[47] Santhosh Kumar Ramakrishnan, Aaron Gokaslan, Erik Wijsmans, Oleksandr Maksymets, Alexander Clegg, John M Turner, Eric Undersander, Wojciech Galuba, Andrew Westbury, Angel X Chang, Manolis Savva, Yili Zhao, and Dhruv Batra. Habitat-Matterport 3D Dataset (HM3D): 1000 Large-scale 3D Environments for Embodied AI. In *NeurIPS*, 2021. 2

[48] Ashutosh Saxena, Min Sun, and Andrew Ng. Make3D: Learning 3D Scene Structure from a Single Still Image. In *TPAMI*, 2009. 8

[49] Johannes Lutz Schönberger and Jan-Michael Frahm. Structure-from-Motion Revisited. In *CVPR*, 2016. 1, 3, 9

[50] Ramprasaath R. Selvaraju, Michael Cogswell, Abhishek Das, Ramakrishna Vedantam, Devi Parikh, and Dhruv Batra. Grad-CAM: Visual Explanations from Deep Networks via Gradient-Based Localization. *IJCV*, 128(2):336–359, 2019. 9

[51] Cameron Smith, David Charatan, Ayush Tewari, and Vincent Sitzmann. FlowMap: High-Quality Camera Poses, Intrinsics, and Depth via Gradient Descent. In *3DV*, 2025. 3, 9, 11, 13

[52] Luming Tang, Menglin Jia, Qianqian Wang, Cheng Perng Phoo, and Bharath Hariharan. Emergent Correspondence from Image Diffusion. In *NeurIPS*, 2023. 12

[53] Ashish Vaswani, Noam Shazeer, Niki Parmar, Jakob Uszkoreit, Llion Jones, Aidan N Gomez, Łukasz Kaiser, and Illia Polosukhin. Attention is All you Need. In *NeurIPS*, 2017. 9

[54] Jesse Vig. A Multiscale Visualization of Attention in the Transformer Model. In *Proceedings of the 57th Annual Meeting of the Association for Computational Linguistics: System Demonstrations*, pages 37–42, 2019. 1

[55] Johannes von Oswald, Eyyvind Niklasson, Ettore Randazzo, João Sacramento, Alexander Mordvintsev, Andrey Zhmoginov, and Max Vladymyrov. Transformers learn in-context by gradient descent. In *ICML*, 2023. 9

[56] Hengyi Wang and Lourdes Agapito. 3D Reconstruction with Spatial Memory. In *3DV*, 2025. 1, 9

[57] Jianyuan Wang, Nikita Karaev, Christian Rupprecht, and David Novotny. VGGSfM: Visual Geometry Grounded Deep Structure From Motion. In *CVPR*, 2024. 3, 9

[58] Qianqian Wang, Yifei Zhang, Aleksander Holynski, Alexei A. Efros, and Angjoo Kanazawa. Continuous 3D Perception Model with Persistent State. In *CVPR*, 2025. 1, 9

[59] Shuzhe Wang, Vincent Leroy, Yohann Cabon, Boris Chidlovskii, and Jerome Revaud. DUSt3R: Geometric 3D Vision Made Easy. In *CVPR*, 2024. 1, 2, 9, 10, 13

[60] Jianing Yang, Alexander Sax, Kevin J. Liang, Mikael Henaff, Hao Tang, Ang Cao, Joyce Chai, Franziska Meier, and Matt Feiszli. Fast3R: Towards 3D Reconstruction of 1000+ Images in One Forward Pass. In *CVPR*, 2025. 1, 9

[61] Botao Ye, Sifei Liu, Haofei Xu, Xuetong Li, Marc Pollefeys, Ming-Hsuan Yang, and Songyou Peng. No Pose, No Problem: Surprisingly Simple 3D Gaussian Splats from Sparse Unposed Images. In *ICLR*, 2025. 9

[62] Yang You, Yixin Li, Congyue Deng, Yue Wang, and Leonidas Guibas. Multiview Equivariance Improves 3D Correspondence Understanding with Minimal Feature Finetuning. In *ICLR*, 2025. 10

[63] Guanqi Zhan, Chuanxia Zheng, Weidi Xie, and Andrew Zisserman. A General Protocol to Probe Large Vision Models for 3D Physical Understanding. In *NeurIPS*, 2024. 10

[64] Junyi Zhang, Charles Herrmann, Junhwa Hur, Varun Jampani, Trevor Darrell, Forrester Cole, Deqing Sun, and Ming-Hsuan Yang. MonST3R: A Simple Approach for Estimating Geometry in the Presence of Motion. In *ICLR*, 2025. 1, 9

[65] Ziqian Zhong, Ziming Liu, Max Tegmark, and Jacob Andreas. The Clock and the Pizza: Two Stories in Mechanistic Explanation of Neural Networks. In *NeurIPS*, 2023. 9

[66] Roland S. Zimmermann, Thomas Klein, and Wieland Brendel. Scale Alone Does not Improve Mechanistic Interpretability in Vision Models. In *NeurIPS*, 2023. 1

## Appendix

### A. Ablations

**Probing head parameterization** Traditionally, 3D probing has been performed by investigating depths and normals [17]. However, the pointmaps from both views must share a common scale for joint visualization. To enforce this, we trained a metric depth probe for each view (see Section E.4 for details), performed scale-shift alignment of the predicted depth maps using least squares, and compared the relative depth accuracy of the metric depth probe against the depth extracted from pointmaps on our test set (Table 1). We report the *absrel* [48] and  $\delta_1$  [29] relative depth metrics. The metric depth probe performs significantly worse, likely due to the scale-invariance of DUS3R features, which negatively impacts the training of metric depth probes. Therefore, for scale-sensitive visualization, the pointmap parametrization is superior.

| Place    | $\delta_1 \uparrow$ |              | absrel $\downarrow$ |              |
|----------|---------------------|--------------|---------------------|--------------|
|          | Depth               | Ptmap        | Depth               | Ptmap        |
| Block 0  | 0.825               | <b>0.937</b> | 0.140               | <b>0.077</b> |
| Block 6  | 0.862               | <b>0.968</b> | 0.124               | <b>0.047</b> |
| Block 11 | 0.795               | <b>0.975</b> | 0.149               | <b>0.038</b> |

Table 1. **Depth estimation performance** across first-view decoder blocks. We compare depth probed from patch tokens (Depth) with depth derived from probed pointmaps (Ptmap).

**Probe capacity** Our head is parameterized by a 5-layer MLP with ReLU activations. We find that it yields considerably cleaner and more interpretable pointmaps compared to the linear head. This also results in a faster decrease of the scale-shift invariant pointmap error over the blocks, as reported in Figure 6. To ablate the role of MLP capacity, we vary the MLP depth but find that using more than 5 layers does not affect the results.

**Probing granularity** We verify the hypothesis of skip connections as a state carrier by probing the direct outputs of every individual layers before skip connections. Figure 7 shows the comparison of scale-shift invariant pointmap error when probed from the skip connection versus when probed directly at the output of the layer. The error after skip connections is clearly more stable. Our visualization in Figure 8 also shows that the direct outputs are less interpretable by pointmap probing. This indicates that the individual layers alter the state in a way that does not necessarily have clear geometric meaning, while the state update from the skip connection does.

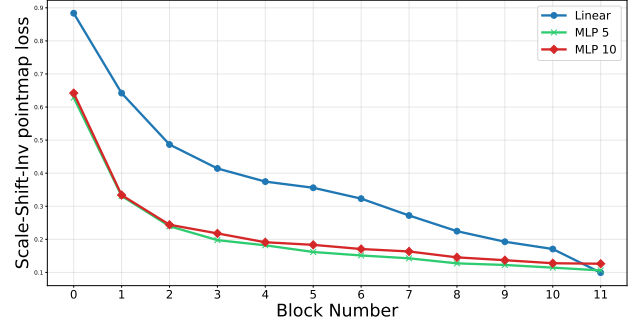


Figure 6. **Ablation study on probing head strength.** We measure a scale and shift-invariant pointmap error at the outputs of the decoder blocks for the second view, comparing different probing head architectures and capacities.

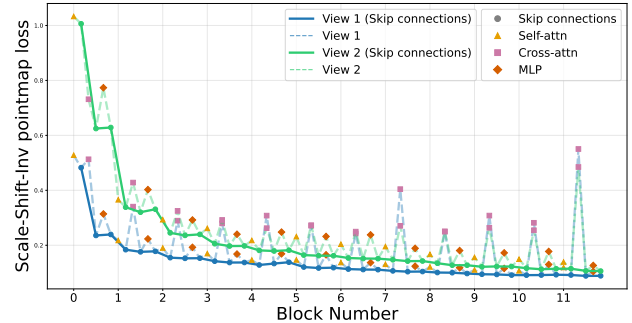


Figure 7. **Probing granularity ablation.** We measure the scale-shift-invariant error on the rendered dataset. We plot the error at the output of each layer (dashed) and after skip connections (solid). The error decreases almost monotonically after skip connections, while other operations exhibit more irregular variations.

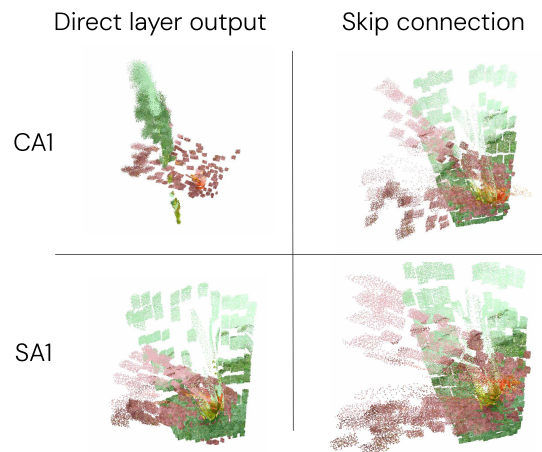


Figure 8. **Visual comparison of pointmaps** probed after skip connections vs direct layer outputs. We observe that probing after skip connections yields clearer and more interpretable geometry.

## B. Related work

### B.1. 3D reconstruction from images

Reconstructing 3D scenes from a set of images is a well-studied problem [26]. Classical Structure-from-Motion (SfM) methods, such as COLMAP [49], solve the unposed 3D reconstruction problem by first establishing a set of correspondences between views. Afterwards, a rough relative camera pose is established and the 3D points are computed based on the camera pose. Finally, coarsely initialized poses and geometry are jointly optimized.

Recently, several attempts were made to replace or enhance this pipeline with deep learning [9, 51, 57, 59]. These approaches typically replace some components of the SfM pipeline with the hope of leveraging data priors for improved robustness or rapidity. By incorporating learned modules in the reconstruction pipeline, they however lose theoretical guarantees and overall interpretability.

Among these, DUS3R [59] marks a significant departure from previous deep and classical approaches. It trains a vision transformer [16, 53] end-to-end to reconstruct a 3D scene from two input views. By doing so, it differentiates itself from classical SfM approaches that often frame the 3D reconstruction problem as an iterative optimization problem. By replacing the entire SfM pipeline with a generic transformer that reconstructs the scene in a feed-forward manner, it also diverges from prior deep methods that only substituted certain components with learned modules while relying on strong handcrafted 3D inductive biases.

Its significant robustness compared to other deep methods motivated follow-up works extending it to 3D reconstruction from more than two images [31, 56, 58, 60]. The concept was further extended to dynamic scene reconstruction [28, 64], novel view synthesis [61], 3D understanding [20], and integrated as a critical block in recent SLAM pipelines [40].

### B.2. Understanding transformers

The transformer [53] is a generic architecture that has been successfully applied across many domains. A large body of ongoing work seeks to understand their features as well as the algorithms and mechanisms they learn [7]. Theoretical works investigate reduced transformer variants and describe how these networks perform operations such as in-context learning [55] or what algorithms they learn when dealing with toy problems such as modular addition [65]. However, most of these attempts have only studied simplified architectures of small models.

Several works build on properties of skip connections that frame the forward pass of residual networks as an iterative process [27]. This view enables us to see the transformer as a process where a state is iteratively updated through the skip connections [13, 23, 39]. The develop-

ment of the internal state across blocks was studied in [6] by probing each block and visualizing the entropy over the most probable tokens. However, visualizing the large discrete token space is not straightforward.

Probing has also been applied at individual layers to inspect the content of features inside various units of the networks, without observing state flow. The quality of features was evaluated on downstream tasks such as classification [1]. At a finer level, sparse probing [25] has been used to identify which neurons are crucial for a given feature.

Sparse autoencoders (SAEs) are a recent and popular method [10, 32]. They aim to disentangle activations at individual layers by imposing sparsity constraints in order to identify interpretable features. SAEs have also been applied to investigate internal state development, but the disentangled representations were found to be very unstable across blocks [30].

Another family of methods enables causal intervention in the computation. Attention knockout [24] and patching interventions [37, 38] are popular approaches that interfere with the computation and compare the results of clean and modified inference.

The success of Vision Transformers (ViTs) [16] motivated ViT-specific methods to understand the interactions between individual patches, for example by visualizing patch-to-patch interactions with an uncertainty-aware framework [34]. Tokens that are attended to by all other tokens in the attention mechanism have been identified in many vision transformers [14], and are suspected to store global information. We also identify these tokens in DUS3R and analyze their role in the 3D reconstruction task.

### B.3. Vision model interpretability

Research on interpreting ViTs is part of a broader field that aims to understand how deep neural networks process images. Several approaches leverage interpretable image visualizations, such as gradient backpropagation to the input space [50], optimized inputs that maximize activations [19, 42], and image reconstructions from features [15, 35].

Beyond visualization, many quantitative methods have been developed to study the role of different units within neural networks. Significant work has focused on understanding both the role of intermediate layers and the information contained in their features, for instance by training linear probes to classify images from features [1]. While these methods enable a local understanding of neural networks, researchers have sought to understand their behavior in greater detail by investigating the role of groups of neurons. Notable work in this direction includes analyzing how manipulating groups of units controls GAN generation and image classification results [4, 5].

Instead of relying solely on images to interpret vision models, multi-modal approaches have recently emerged as a means to study image representations. Alignment with textual embeddings has become particularly prominent, as it is readily available in vision–language models [3, 21] and can also be learned through a linear mapping for uni-modal vision encoders [2].

The 3D awareness of vision models has also been thoroughly evaluated. 3D understanding is necessary for a wide range of vision tasks, which has motivated several works to evaluate this capacity in vision models [17, 36, 63]. This evaluation has, in turn, motivated further improvements in 3D-aware fine-tuning strategies [62]. In this work, we extend this line of research by analyzing DUS3R [59], a feed-forward image-to-3D model.

<https://arxiv.org/abs/2012.09838>

## C. Training Details

**Optimizer** We use the AdamW optimizer [33] with a learning rate of 1e-4 and a weight decay of 0.05.

**Supervision** The probes are supervised via a confidence-weighted 3D regression loss introduced in DUS3R [59]. For a view  $v \in \{1, 2\}$ , let  $\bar{X}^{(v)}$  denote the ground-truth pointmap provided over a subset of valid pixels

$$D^{(v)} \subseteq \{1, \dots, W\} \times \{1, \dots, H\}.$$

We first normalize both the predicted and ground-truth pointmaps by their respective scale factors:

$$z = \text{norm}(X^{(v)}) \quad \text{and} \quad \bar{z} = \text{norm}(\bar{X}^{(v)}),$$

where

$$\text{norm}(X^{(v)}) = \frac{1}{|D|} \sum_{(i,j) \in D} \|X_{i,j}^{(v)}\|_2.$$

A per-pixel regression loss is then defined as

$$\ell_{\text{regr}}^{(v)}(i, j) = \left\| \frac{X_{i,j}^{(v)}}{z} - \frac{\bar{X}_{i,j}^{(v)}}{\bar{z}} \right\|_2. \quad (1)$$

The final loss, computed over both views  $v \in \{1, 2\}$  expressed in first-view coordinate system is given by

$$L = \sum_{v \in \{1, 2\}} \sum_{(i,j) \in D^{(v)}} \left[ C_{i,j}^{(v)} \ell_{\text{regr}}^{(v)}(i, j) - \alpha \log(C_{i,j}^{(v)}) \right], \quad (2)$$

where  $\alpha$  is a weighting hyperparameter that regularizes the confidence, and  $D^{(v)}$  denotes the valid pixels in view  $v$ . We use  $\alpha = 0.2$  in our experiments. Confidence scores are learned without explicit supervision. Each pixel's confidence value  $C_{i,j}^{(v)}$  modulates the loss to reduce the impact of unreliable or ambiguous predictions (e.g., sky or translucent regions).

## D. Further visualizations

We present a motivating example in Figure 9, illustrating how correspondences are refined from semantic to geometric across decoder blocks. Additional pointmap visualizations for early decoder blocks are provided in Figure 10, along with colored refinement examples in Figure 11.

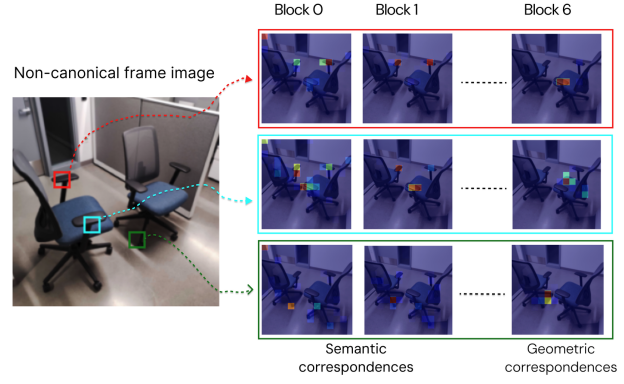


**Figure 9. Correspondence geometric refinement.** We show cross-attention maps for query patches (colored) from the left image. Red indicates the highest activation, and blue the lowest. The selected heads produce sharply peaked attention maps: early layers attend to semantically similar regions (e.g., different armrests are not distinguished), while later layers focus on the geometrically corresponding patches in the other view.

## E. Additional probing details

### E.1. Details on the scale-shift invariant error

Following [59], we measure a scale–shift invariant error. Intuitively, this corresponds to an L2 error on normalized pointmaps. Formally, let  $X \in \mathbb{R}^{H \times W \times 3}$  denote a predicted pointmap. The pointmap is first made invariant to depth shift. We compute its median depth  $z_{\text{med}}$  and subtract it from the depth of every vector  $X_{i,j} \in \mathbb{R}^3$ :

$$\tilde{X}_{i,j,z} = X_{i,j,z} - z_{\text{med}}.$$

The same operation is applied to the ground-truth pointmap. Next, the pointmaps are made invariant to scale variations. From the shift-invariant pointmaps, we compute the coordinate-wise median across all 3D points (from both views), which serves as the origin for scale normalization. The scale  $s_{\text{med}} \in \mathbb{R}$  of a pointmap is then defined as the median norm of its 3D points relative to this origin. The ground-truth scale  $\bar{s}_{\text{med}} \in \mathbb{R}$  is estimated in the same way. The predicted pointmap is then rescaled to match the ground-truth scale:

$$S = \frac{\bar{s}_{\text{med}}}{s_{\text{med}}} \tilde{X} \in \mathbb{R}^{H \times W \times 3}.$$

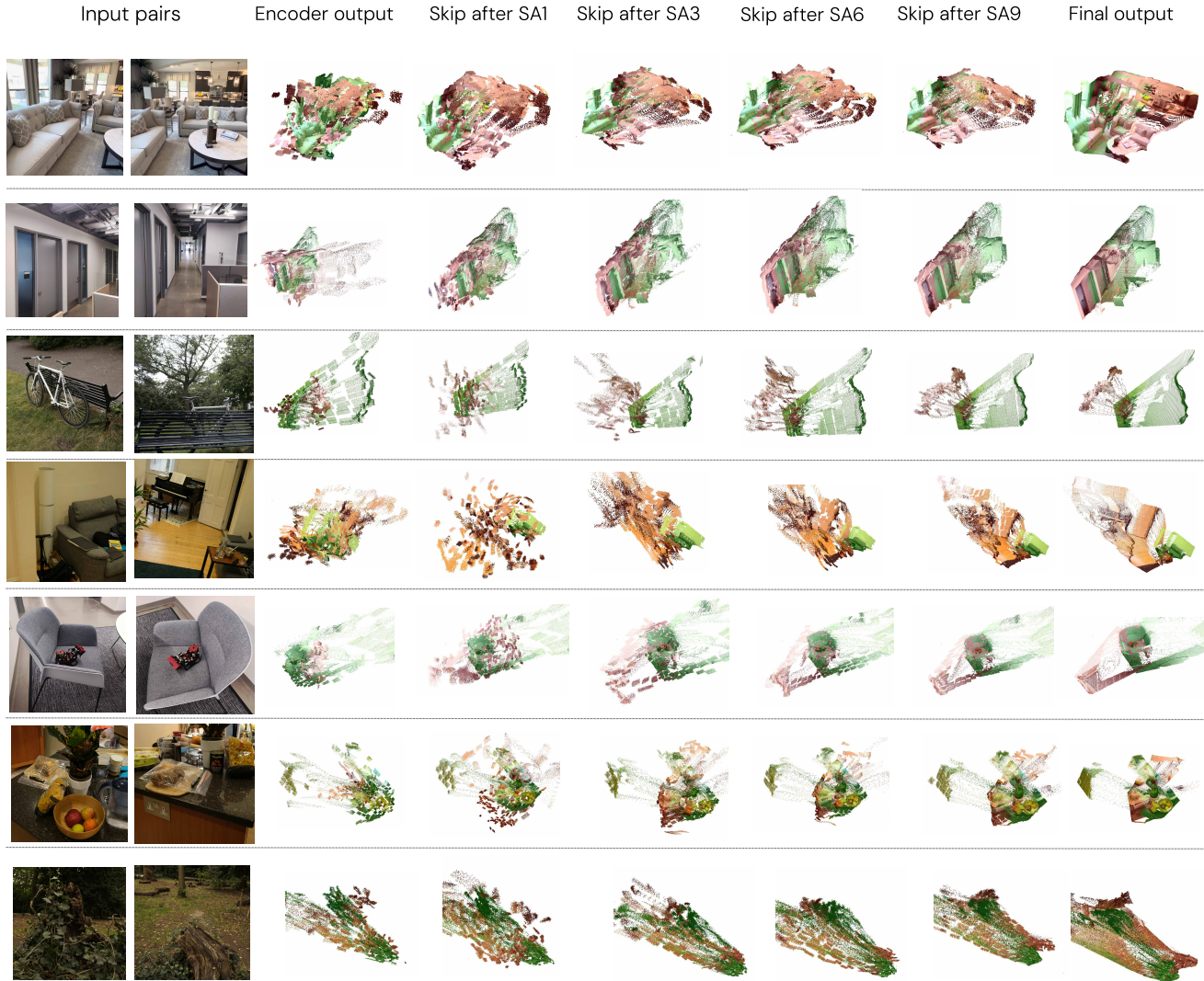


Figure 10. **Additional pointmap visualizations.** The two simpler top scenes (room and corridor) converge after a single cross- and self-attention iteration. The four more challenging bottom cases (bicycle, couch corner, chair with Lego, counter) require 3–6 iterations to correctly align the second-view patches (red). In the final opposing-view example (stump), reconstruction fails, likely due to early convergence to a local minimum.

Denoting the ground-truth shift-invariant pointmap (without rescaling) as  $\bar{S}^{(v)}$ , the per-pixel scale–shift invariant error for view  $v \in \{1, 2\}$  is defined as a per-vector L2 loss:

$$\ell_{\text{ss\_inv\_regr}}^{(v)}(i, j) = \left\| S_{i,j}^{(v)} - \bar{S}_{i,j}^{(v)} \right\|_2. \quad (3)$$

Finally, the overall scale–shift invariant pointmap error is given by:

$$L = \sum_{v \in \{1, 2\}} \sum_{(i,j) \in D^{(v)}} \ell_{\text{ss\_inv\_regr}}^{(v)}(i, j). \quad (4)$$

## E.2. Intra-view geometry of the second view

We extract the predicted and ground-truth second-view pointmaps  $X^{(2)}, \bar{X}^{(2)} \in \mathbb{R}^{H \times W \times 3}$ , and align them via a Procrustes following [51]. This solves for the optimal rigid transformation in the weighted Procrustes problem:

$$\arg \min_{P \in SE(3)} \| W^{1/2} (X^{(2)} - P \bar{X}^{(2)}) \|_2^2, \quad (5)$$

where  $W$  contains the predicted confidences for the second view and is used as correspondence weights. The predicted pointmap is then aligned to the ground-truth using the optimal transformation, and the scale–shift invariant error described above is computed. To ensure that the shift

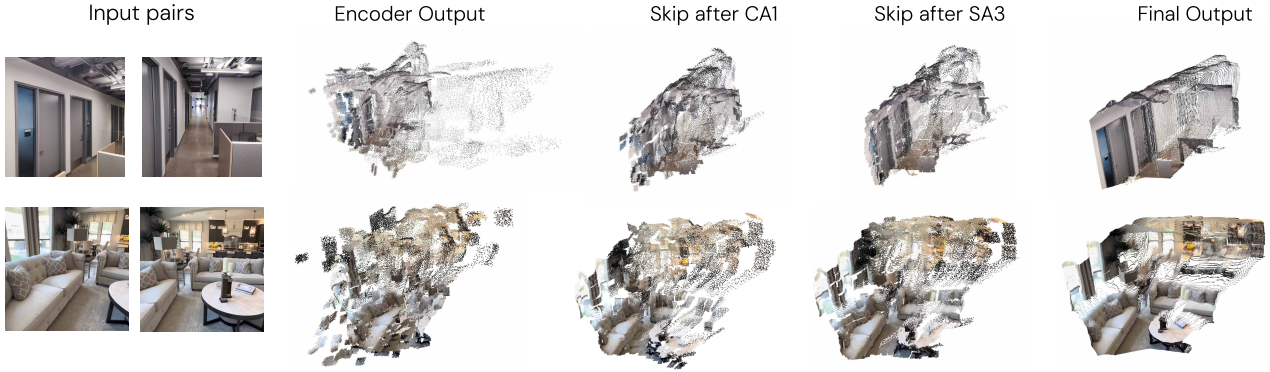


Figure 11. Additional visual examples with RGB colors.

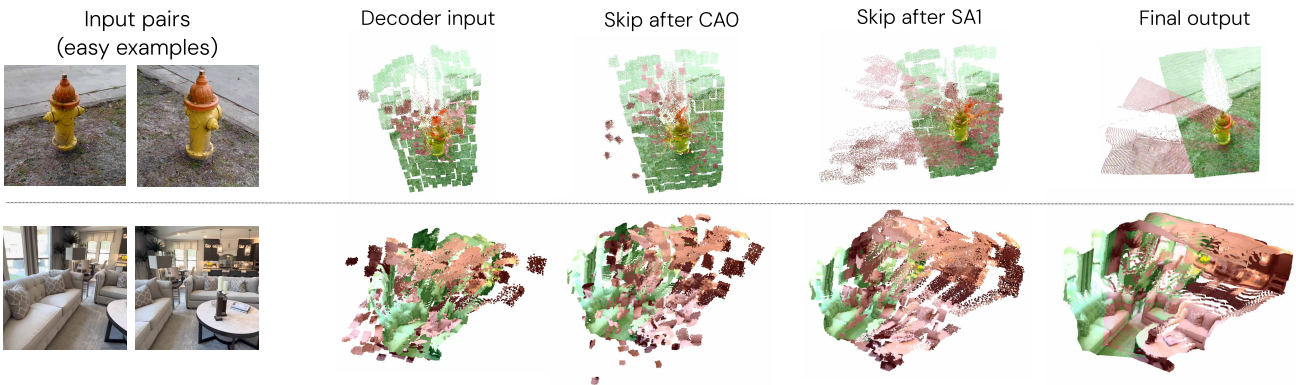


Figure 12. **Visualization of probed pointmaps for early decoder blocks.** We visualize pointmaps on easy samples after the first few cross-attention and self-attention layers in the decoder. We also include the encoder output and the final output for reference. The first view is tinted green, and the second is tinted red. These results highlight the role of the self-attention layer in restoring the intra-view geometry of the second view.

and normalization operations remain consistent after Procrustes alignment, we discard the first view. We then set  $X^{(1)} = X^{(2)}$  during shift and normalization, and report the error only on the second view.

### E.3. Correspondence probing

Following [17, 52], we probe correspondences in a zero-shot setting. Instead of using feature similarity as in their approach, we extract correspondences from the cross-attention maps of the second-view decoder. This is motivated by our observation (Figure 9 and Section F.2) that several cross-attention heads act as correspondence heads. For each identified correspondence head  $h$ , we estimate correspondences as follows.

For each query patch  $p^2$  in the second view that has a ground-truth correspondence, we predict its correspondence by computing the arg max over the attention map  $A_h$ :

$$\hat{p} = \arg \max_{p^1} A_h(p^2, p^1),$$

where  $p^1$  indexes patches in the first view. In other words,

we select the patch in the first view with the highest attention score for the query token associated to  $p^2$ . Following [17], we measure the correspondence error as the Euclidean distance between the centers (in pixel coordinates) of the predicted and ground-truth corresponding patches. Since the evaluation operates at the patch level, this results in a coarse measure of correspondence recall.

For each layer, we evaluate the correspondence quality of every head and select the best-performing one as our estimator.

**Obtaining ground-truth patch correspondences** We extract dense pixel correspondences from our rendered dataset. Because the attention maps are at a lower resolution ( $14 \times 14$ ), we downsample to patch-level correspondences by defining the corresponding patch in the other view as the one containing the largest number of corresponding pixels. Although this mapping is not strictly bijective, we found it to be a good approximation in practice.

## E.4. Depth probing

For depth probing with a specialized metric depth head, we use a 5-layer MLP followed by a confidence-aware head ( $\alpha = 0.2$ ) that predicts a single depth value. Following [51, 59], the final depth prediction is obtained as

$$d = \exp\left(\frac{x}{c}\right),$$

where  $x$  is the raw output of the head and  $c = 4$ . The choice of  $c = 4$  was made empirically to match the scale of the Habitat Matterport 3D dataset: it allows the network to output values near zero and then map them smoothly into metric depths in the range of roughly 0–10.

## F. Attention maps visualizations

### F.1. Self-attention

We visualize self-attention maps in the second decoder block of the second view for the hydrant example in Figure 14. We selected this layer because it contributed most to reducing the second-view pointmap error after Procrustes alignment (see Figure 4a). We identify heads that mainly attend to neighboring patches of the query and others that consistently attend to a fixed subset of patch tokens across all queries. We refer to these heads as *register heads* and these subsets of tokens as *register tokens*, which likely correspond to the high-norm tokens identified in [14]. Note that our use of this term differs from their paper, where it refers to additional tokens introduced to overcome this phenomenon. This behavior repeats across samples and can also be observed in other decoder blocks; however, we show only one block on a single example for brevity.

### F.2. Cross-attention

We visualize cross-attention maps in the first decoder block for the hydrant example in Figure 15. Similar to self-attention, the attention maps indicate a specialization of individual heads for particular tasks. Noticeably, heads 3, 5, 7, 8, and 11 attend to candidate corresponding patches for the query, whenever correspondences exist. The behavior of these correspondence heads is consistent across samples. We also observe heads attending to *register tokens*, as in the self-attention map. Besides, we notice that cross attention maps tend to be significantly sharper than self-attention ones.

## G. Attention knockout of the register heads

We study the role of register tokens in storing and transmitting global information. To this end, we perform a causal intervention on the network activations of the hydrant example using attention knockout [24]. Specifically, we intervene on the attention maps of the self-attention heads in

the second decoder block, which make the largest contribution to decreasing the second-view pointmap error after Procrustes alignment (see Figure 4a). We focus on heads 0, 3, 8, and 9, which attend exclusively to the register tokens regardless of the query, as identified in Figure 14. In particular, we prevent information transfer from the register tokens to the other patch tokens by zeroing out the self-attention activations of the five tokens with the largest values, which should correspond to registers. The probe output after intervention, visualized in Figure 13, shows almost no difference from the pointmap obtained without intervention.

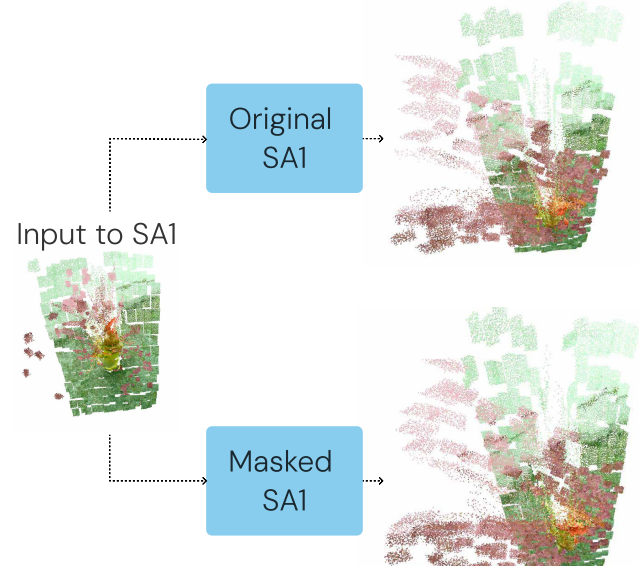


Figure 13. **Study of the global role of registers via an attention knockout.** In the self-attention mechanism of the second block of the second-view decoder, we mask the five tokens receiving the highest attention in the heads identified as *registers* (heads 0, 3, 8, and 9). We show the pointmap probe before the layer (left), the output without this intervention (top right) and with this intervention (bottom right). The probe output remains unaffected by the masking operation, suggesting that these *register tokens* do not store global information, including pose.

Since this layer makes a significant contribution to restoring global geometry within the second view, this highlights that register tokens do not play an essential role in storing and transmitting global information in the self-attention mechanism.

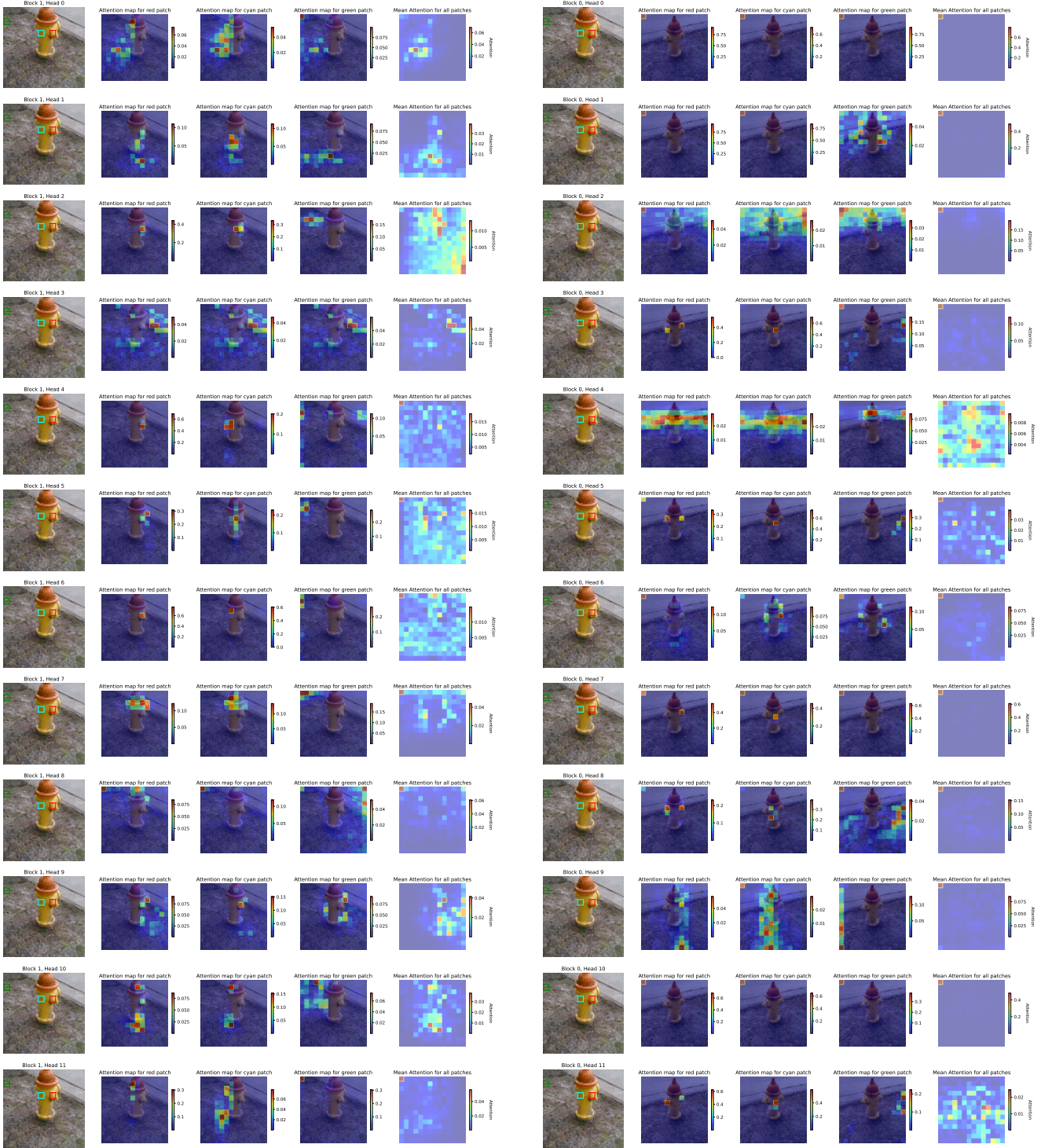


Figure 14. **Visualization of self-attention maps** in the second decoder block of the second view. We visualize the attention maps for three query patches shown on the query image. Heads 1, 2, 4, 5, 6, and 11 mainly attend to local patches around the query; heads 0, 3, 8, and 9 are identified as attending to *register tokens*. The locations of these registers vary across examples.

Figure 15. **Visualization of cross-attention maps** in the first decoder block of the second view. We visualize the attention maps for three query patches shown on the query image. Heads 3, 5, 7, 8, and 11 act as correspondence heads, while heads 0, 3, 8, and 10 consistently attend to the top-left *register token*. Heads 9 and 4 exhibit spatial behavior, performing vertical and horizontal searches, respectively.